Nanomed Res J 7(2):173-188, Spring 2022

RESEARCH ARTICLE

Zinc TetraPhenylPorphyrin / Dextran-Graft-PolyAcrylAmide / Gold Nanoparticles Hybrid Nanosystem for Photodynamic Therapy: Plasmonic Enhancement Effect

Oleg A. Yeshchenko[1*], Nataliya V. Kutsevol [1],Anastasiya V. Tomchuk [1], Pavlo S. Khort [1], Pavlo A. Virych [1], Vasyl A. Chumachenko [1],Yulia I. Kuziv[1], Antonina P. Naumenko [1],Andrey I. Marinin[2]

[1] Physics Department and Chemistry Department, Taras Shevchenko National University of Kyiv, 60 Volodymyrs'ka str., 01601 Kyiv, Ukraine

[2] Problem Research Laboratory, National University of Food Technology, 68Volodymyrska str., 01601 Kyiv, Ukraine

ARTICLE INFO

Article History:
Received 20 January 2022
Accepted 05 April 2022
Published 01 May 2022

Keywords:
Gold nanoparticles
Polymer
Photosensitizer
Hybrid nanosystem
Surface plasmon enhancement,
Photodynamic Therapy

ABSTRACT

Objective(s): In recent years, great attention towards alternative antitumor and antibacterial therapies such as antibacterial photodynamic therapy (PDT) has been raised. The development of nanotechnology has opened wide opportunities for the creation of new multifunctional hybrid multicomponent nanosystems with high potential for PDT applications. In particular, those are the Photosensitizer / Polymer / Metal nanoparticles nanosystems containing the photosensitizer as a drug, polymer as a drug nanocarrier, and metal nanoparticles as an enhancer of drug efficiency.

Methods: The Zinc TetraPhenylPorphyrin photosensitizer / Dextran-graft-PolyAcrylAmide copolymer / Au NanoParticles (ZnTPP/D-g-PAA/AuNPs) triple hybrid nanosystem were synthesized in water solution as a nanodrug for potential use in PDT applications. Dynamic light scattering has proved the aggregation and sedimentation stability of this system during several days after preparation. The absorption and fluorescence spectra of ZnTPP/D-g-PAA/AuNPs water solution have proved the binding of ZnTPP molecules with both D-g-PAA and D-g-PAA/AuNPs macromolecules.

Results: The gold concentration of 0.005 mg/mL was shown to be optimal providing the highest plasmonic enhancement of the electronic processes involving the ZnTPP photosensitizer. The 3.2 times enhancement of singlet oxygen photogeneration under resonant with localized surface plasmon wavelength excitation has been detected for ZnTPP/D-g-PAA/AuNPs that proves the plasmonic origin of such phenomenon. The high bactericidal efficiency of ZnTPP/D-g-PAA/AuNPs water solution at 530 nm light irradiation was revealed for wild strains *of Staphylococcus aureus*.

Conclusions: These data indicate that ZnTPP/D-g-PAA/AuNPs hybrid nanosystem is quite promising for rapid antibacterial photodynamic therapy, the open wounds in particular.

How to cite this article
Yeshchenko O.A., Kutsevol N.V., Tomchuk A.V., Khort P.S., Virych P.A., Chumachenko V.A., Kuziv Y.I., Naumenko A.P., Marinin A.I. Zinc TetraPhenylPorphyrin / Dextran-Graft-PolyAcrylAmide / Gold Nanoparticles Hybrid Nanosystem for Photodynamic Therapy: Plasmonic Enhancement Effect. Nanomed Res J, 2022; 7(2): 173-188. DOI: 10.22034/nmrj.2022.02.007

INTRODUCTION

The growing resistance of pathogenic bacteria to many antibiotics and the emergence of multidrug-resistant bacteria indicate the inevitability of a "post-antibiotic era" [1]. Therefore, the great interest to alternative antibacterial therapies such as antibacterial photodynamic therapy (PDT) has raised. The light responsive agents - photosensitizers (PS) play a central role in antibacterial PDT method. The PS usually applied in an oxygen-rich environment [2,3]. Recent literature data testify that antibacterial PDT can be effective alternative to antibiotics while having a number of advantages: i) antibacterial effect is independent of antibiotic resistance; ii) more limited harmful effect to host tissue; iii) no resistance after many antibacterial PDT sessions. In antibacterial PDT

* Corresponding Author Email: *yes@univ.kiev.ua*

method, the light irradiated PS produce singlet oxygen and free radicals which have killing effect on microorganisms [4].

Nowadays, the most effective PSs used in PDT including antibacterial and antitumor therapy are based on porphyrin and its derivatives [5,6]. The advantages of porphyrins as photosensitizers are the stability, strong absorption of light in VIS range, high efficiency of singlet oxygen photogeneration, easy functional modification, long lifetime in triplet state, low dark toxicity, etc. Unfortunately, the vast majority of PSs are hydrophobic, that caused their aggregation in biological environments that leads to a reduction in their photochemical efficiency [6]. Recently, metalloporphyrins has attract high interest. Due to the paramagnetic effect, the PDT efficiency of PS metal complexes depends on the certain metal [7]. The addition of zinc into the porphyrin ring allows to increase the stability of porphyrin ring and to maintain the photophysical activity of PS. The zinc containing porphyrins, e.g. zinc tetraphenylporphyrin (ZnTPP), are more similar to natural porphyrin than *meso*-substituted porphyrins. The ZnTPP is widely used in biological studies and applications. There are reports that the presence of zinc in porphyrin ring reduces binding to mitochondria and promotes binding to membranes which is due to the complexation with phospholipid phosphate groups. Such mechanisms result in increasing of photodynamic efficiency [8].

Recently, a high anticancer efficiency was revealed for several gold-based compounds [9,10]. It is well known that gold nanoparticles (Au NPs) are widely used in immense biological applications. Gold NPs have lower toxicity than silver NPs [11,12]. Also, there is great potential for the use of the localized surface plasmon resonance (LSPR) in Au NPs. In particular, the collective coherent oscillations of free electrons in metal NP arising at LSPR excitation cause frequency dependent photothermal effect (plasmonic heating). The plasmonic heating has a prominent resonant character becoming especially pronounced when the frequencies of incident light and LSPR are in close proximity [13–15]. Since metals have a very low quantum yield of the fluorescence, almost all of absorbed energy of light is conversed into heat. Thus, the metal NPs act as highly efficient heat nanosources. Therefore, the plasmonic heating is making metal NPs suitable for photothermal treatment of cancer and bacterial diseases [16–19]. Another plasmon involving effect useful for PDT applications is a plasmonic enhancement effect. The surface plasmonic oscillations of free electrons in metal NP generate of a very intense local electric field in proximity of the NP surface. Such intense local field enhances strongly the electronic processes in molecules functionalized on the surface of nanosized metal, e.g. Raman scattering (SERS), absorption (SEA), fluorescence (SEF), photocatalysis, etc. [20–22]. The plasmonic enhancement of light absorption by PS molecules located in proximity of the metal NP surface should increase the yield of singlet oxygen that should increase the PDT efficiency of the hybrid nanosystem containing the PS molecules and metal NPs [23–27]. Also, Au NPs have bactericidal activity against some pathological bacteria [28] that is due to its high cellular penetration caused by its ultra-fine size. In addition, the bactericidal efficiency of the Au NPs can be improved by the plasmonic enhancement of singlet oxygen photogeneration. It was proved that such effect was enhanced by photothermal degradation of such cells. Thus, the laser irradiated Au NPs can be used as effective bactericidal approach. Recently, the high potential of Au NPs has been also shown for the high energy photon radiation therapy of cancer [29–31].

Polymeric nanomaterials are widely used in biomedical research and applications. The use of water soluble biocompatible polymers in nanomedicine applications can provide high bioavailability and pharmacokinetics that has to increase the efficiency of therapeutic agents [32]. Polymers can be used as matrices for convenient and efficient *in situ* synthesis of metal NPs which allows to prevent their aggregation and control the NPs size [33–36]. The unique chemical and biological properties of polymer molecules allow to improve delivery and controlled release of therapeutic agents. The high stability of polymer molecules in the human body provides the optimal biodistribution that allows to protect the healthy tissues and accumulate drugs in the diseased tissue. The encapsulation of PS molecules into polymer matrix allows to prevent an aggregation of hydrophobic PS molecules and, correspondingly, to increase considerably the PDT efficiency of PS [37].

In our paper we present the results of synthesis as well as morphology, optical properties and bactericidal activity of the aqueous solution of ZnTPP / D - g - PAA / Au NPs hybrid nanosystem designed for potential PDT applications. The features of the binding of the photosensitizer zinc

tetraphenylporphyrin molecules to D - g - PAA / Au NPs macromolecules as well as their interaction with polymer D - g - PAA and Au NPs are analyzed. The considerable impact of the LSPR in Au NPs on the light absorption and fluorescence by ZnTPP molecules as well as on the singlet oxygen photogeneration and on the bactericidal activity of the ZnTPP / D - g - PAA / Au NPs nanosystem have been revealed. The high potential of ZnTPP / D - g - PAA / Au NPs nanosystem for the rapid bactericidal PDT of the open wounds has been concluded.

MATERIALS & METHODS

Synthesis of ZnTPP / D - g - PAA and ZnTPP / D - g - PAA / Au NPs hybrid nanosystems

The details of synthesis of Dextran – graft - Polyacrylamide copolymer (D - g - PAA) was given in Ref. [38]. Herein, we used D - g - PAA with average molecular weight of M_w = 1.7×10^6 g·mol^{-1} and polydispersity of M_w/M_n =1.66. The M_w of dextran core was 7×10^4 g·mol^{-1} and the average number of PAA grafted chains per dextran molecule was equal to 10. Chemical structure of D - g - PAA macromolecule and its schematic representation is shown in Fig. 1. The synthesized polymer is star-like. The D - g - PAA macromolecule is more rigid and compact with higher local concentration of functional groups than linear PAA. It results in high efficiency of D - g - PAA polymer matrix for in situ synthesis of metal NPs and obtaining stable in time nanosystems [38].

Au NPs were synthesized by $HAuCl_4$ reduction (gold precursor) dissolved in solution of D - g - PAA polymer. 0.05 mL of $HAuCl_4$ aqueous solution with c = 0.1 M concentration was mixed with 1 mL of aqueous solution of D - g - PAA polymer with c = 1 g/L and stirred for 20 min. Then, 0.1 mL of $NaBH_4$ aqueous solution with c = 0.1 M was added. The obtained solution was stirred for 30 min. It became ruby-red in color that indicated the formation of Au NPs.

The stock ethanol solution of Zinc tetraphenylporphyrin (ZnTPP) of concentration 0.1 g/L was prepared at 40 ^{0}C. The stock solutions of D - g - PAA (c = 1 g/L) and D - g - PAA / Au NPs ($c_{D\text{ - }g\text{ - }PAA}$ = 0.8696 g/L and c_{Au} = 0.8565 g/L) were prepared by dissolving in water at 20 ^{0}C. Then, 0.03 mL of ZnTPP ethanol solution (c = 0.1 g/L) was mixed with 2.97 mL of diluted aqueous solutions of D - g - PAA or D - g - PAA / Au NPs. Finally, the aqueous solutions of ZnTPP / D - g - PAA or ZnTPP / D - g - PAA / Au NPs composite nanosystems of various concentrations were obtained. The ZnTPP concentration was equal to 0.001 g/L for all samples.

Morphology and size characterization by TEM and DLS

Transmission electron microscopy (TEM) measurements were carried out to study the morphology of the studied hybrid nanosystems. TEM measurements were carried out by a Tecnai G2 microscope (FEI) and the images were acquired by a ssCCD Eagle camera. The TEM measurements were performed at room temperature.

Since TEM does not allow to determine the morphology and size characteristics of the polymer and photosensitizer components in the hybrid

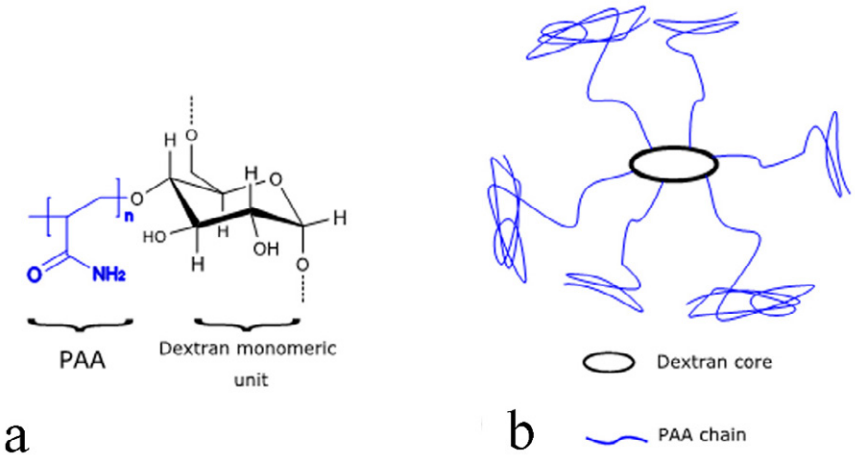

Fig. 1. (a) – Chemical structure of D - g - PAA copolymer and (b) – schematic representation of D - g - PAA macromolecule.

nanosystem, we used the dynamic light scattering (DLS) method. The hydrodynamic particle size distribution (PSD) for studied aqueous solution was measured using the dynamic light scattering (DLS) method by Zetasizer Nano-ZS90 (Malvern Panalytical) equipped with a 5 mW He-Ne laser. The DLS measurements were performed in backscattering geometry at scattering angle of 173°. PSD were obtained from autocorrelation functions using method based on nonnegative truncated singular value decomposition [39]. The DLS measurements were carried out at room temperature.

Optical spectroscopy

The light absorption spectra were measured by a Cary 60 UV-VIS spectrophotometer (Agilent). The FL spectra were measured by a Shimadzu RF-6000 spectrofluorophotometer (Shimadzu). The singlet oxygen emission spectra were measured by a FluoroMax Plus CP spectrofluorometer (HORIBA). The FL was excited by 421 nm light. The singlet oxygen emission was excited by 421 and 553 nm light. The studied solutions were placed in 1cm´1cm´4cm quartz cell. The optical measurements were performed with time delay from 1 min to 7 days after mixing of ZnTPP in ethanol with water and aqueous solutions of D - g - PAA and D - g - PAA / Au NPs. The spectra were recorded at room temperature.

Biological experiments

The study was performed on *Staphylococcus aureus* (*S. aureus*) wild strains isolated on the salt egg yolk agar of the following composition (g/L): peptone – 10, sodium chloride – 70, heart extract powder – 5, mannitol – 15, agar – 15, pH = 7.3. The sensitivity of microorganisms to the action of ZnTPP / D - g - PAA / Au NPs nanocomposite aqueous solution was investigated in a bacteria suspension, which was prepared in Mueller-Hinton medium (g/L): casein hydrolyzate - 17.5, peptone - 2, water-soluble starch - 1.5, pH = 7.3. The number of colony-forming units (CFU) was $3{\cdot}10^6$ – $4{\cdot}10^6$ per ml. The prepared suspension was divided into 1 mL glass tubes. The bacteria were in water bath for 20 minutes at 37 ^{0}C before experiment. Toxicity of ZnTPP / D - g - PAA / Au NPs and individual components in a suspension of *S. aureus* was tested. The final concentration of ZnTPP was 0.001 g/L, Au NPs – 0.08, 0.008 and 0.0008 g/L. The measurements were carried out with a 5 min interval for 30 minutes. The bactericidal effect was calculated relative to an aliquot of the *S. aureus* suspension under similar conditions. This accounts the rate of reproduction of microorganisms. The number of CFU doubles every 1 – 1.5 hours. The suspension was at 37 °C throughout the experiment.

Medical light therapy LED device LIKA-LED (Photonica Plus) was used for 420, 530 and 660 nm light irradiation of the samples. Power of light irradiation was 0.1 J/s, dose of irradiation was in the range of 3 – 18 J/ml with step of 3 J/ml. The *S. aureus* containing suspension was irradiated for 15 min after adding the hybrid nanocomposite solution. The number of CFUs was determined in Goryaev chamber after staining the suspension with acridine orange ($3.5{\cdot}10^{-3}$ M). Fluorescence was detected by an Olympus BX53 microscope with X-Cite Series 120 Q block and DP72 camera. The statistical processing of obtained results was made by Scheffe (ANOVA, $p<0.05$) and Shapiro-Wilk ($p>0.05$) tests. The experiments were iterated three times.

RESULTS AND DISCUSSION

Morphology and size study

The examples of D - g - PAA / Au NPs nanosystem TEM images are shown in Fig. 2. The Au NPs are spherical and have radius of 2.8 ± 0.8 nm. Let us note that the polymer is not visible on the TEM images due to considerably lower contrast comparing to metal NPs. However, one can see that Au NPs are arranged mainly in groups, which confirms that in the samples they are predominantly bound to D - g - PAA macromolecules, although some of the Au NPs are free. Also, the ZnTPP molecules are not visible on TEM images due to their small size and low contrast.

Since TEM does not allow to determine the morphology and size characteristics of the polymer and photosensitizer components in the hybrid nanosystem, we used the DLS method. PSD of D - g - PAA, ZnTPP, ZnTPP / D - g - PAA and ZnTPP / D - g - PAA / Au NPs solutions are shown in Fig. 3. DLS measurements of the solutions of supposedly unstable systems (ZnTPP, ZnTPP / D - g - PAA and ZnTPP / D - g - PAA / Au NPs) were carried out in 1 hour, 24 hours and 9 days after the fabrication (mixing). PSD of D - g - PAA includes the single peak corresponding to hydrodynamic radius R_H = 37 nm (Fig. 3(a)). For ZnTPP poorly soluble in water, we observed aggregates with R_H = 32 nm, Fig. 3(b). One can see from Fig. 3(b) that ZnTPP

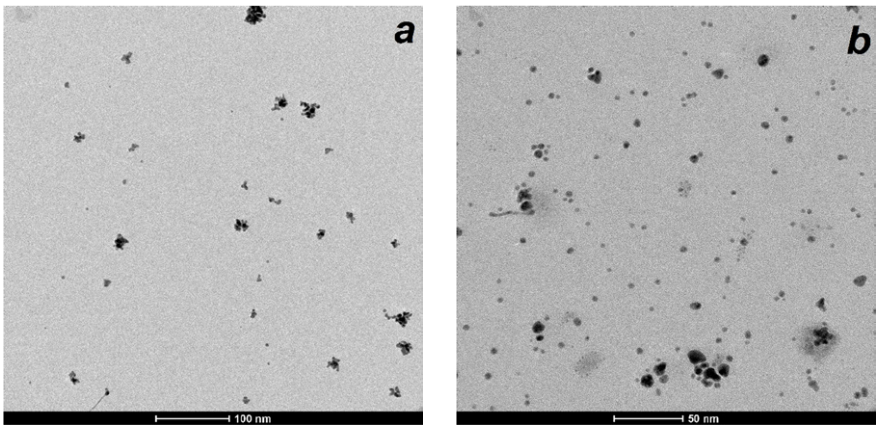

Fig. 2. Typical TEM images of D - g - PAA / Au NPs hybrid nanosystem.

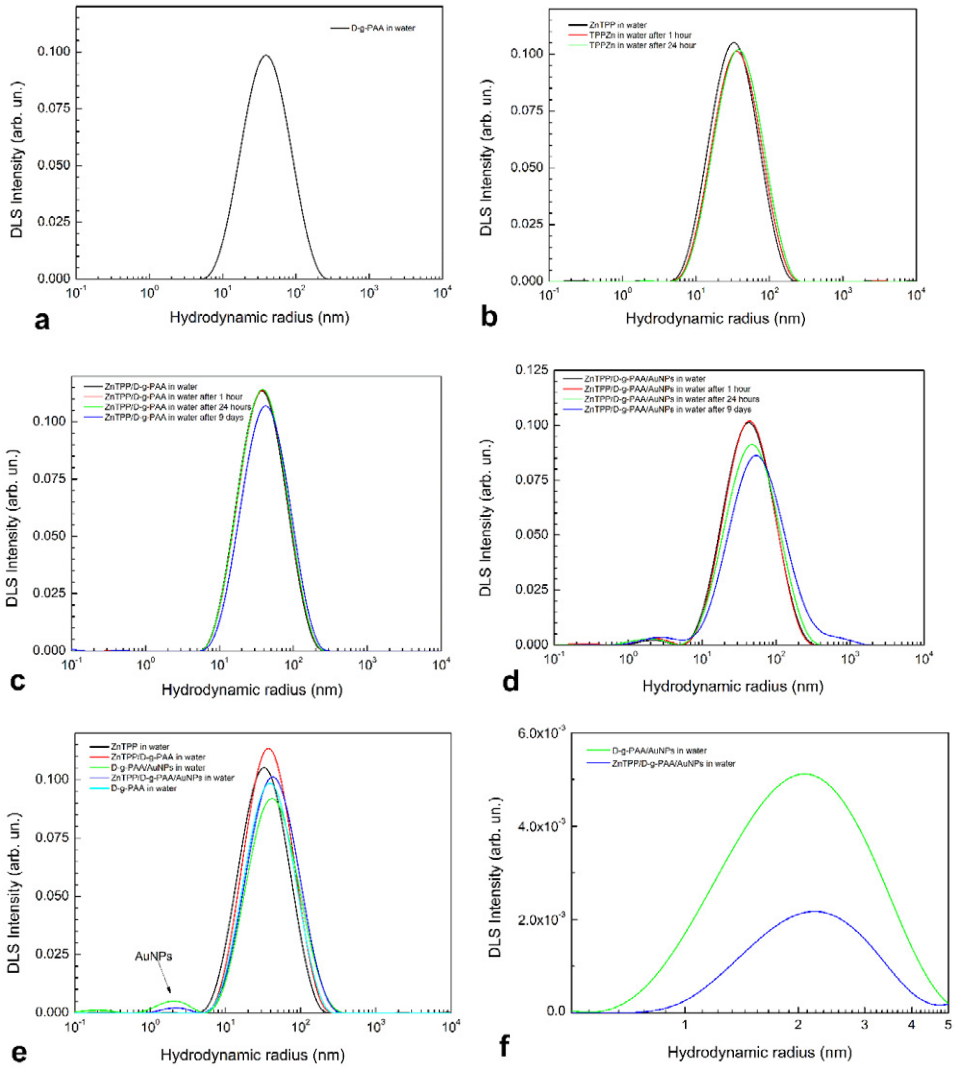

Fig. 3. (a) – PSD of D - g - PAA aqueous solution. PSD of freshly prepared certain aqueous solution and this solution in 1 hour, 24 hours and after 9 days for: (b) – ZnTPP, (c) – ZnTPP / D - g - PAA, (d) – ZnTPP / D - g - PAA / Au NPs. (e) – PSD of freshly prepared D - g - PAA, ZnTPP, ZnTPP / D - g - PAA, D - g - PAA / Au NPs and ZnTPP / D - g - PAA / Au NPs aqueous solutions. (f) – zoom-in of Au NPs peak for D - g - PAA / Au NPs and ZnTPP / D - g - PAA / Au NPs systems.

aqueous solution PSD did not change significantly during time of observation. Only in 9 days, peak shifted slightly to higher radius side. The PSD of ZnTPP and D - g - PAA mixture is similar to the PSDs of free ZnTPP and D - g - PAA having maximum at 38 nm, Fig. 3(c). It is quite expectable considering the close R_H values of separate components of the solution. Also, ZnTPP / D - g - PAA system was revealed to be aggregatively and sedimentationally stable having the maxima at R_H = 38 – 41 nm.

The three component ZnTPP / D - g - PAA / Au NPs system is characterized by two PSD peaks at 3 nm and 44 nm, Fig. 3(d). The first maximum was attributed to Au NPs and the second one to both ZnTPP and D - g - PAA. Let us note the perfect agreement between the mean Au NPs radius obtained by TEM (2.8 nm) and DLS (3 nm) methods. Let us note that despite low intensity of Au NPs PSD peak, the relative number of Au NPs is quite large, since the Rayleigh scattering intensity for small particle is $\propto R_H^6$. After the first day we observed no change in both peaks positions on ZnTPP / D - g - PAA / Au NPs PSD, Fig. 3(d). Only in 9 days, the second peak attributed to ZnTPP / D - g - PAA shifted from 44 to 54 nm and additional peak with low intensity at 650 nm corresponded to large aggregates has appeared, Fig. 3(d).

PSD of each studied system are collected in Fig. 3(e) to make the comparison more convenient. All the systems included one well defined peak at 37 – 44 nm with similar peak width and shape, and only PSD of Au NPs contained systems had the second low intensity peak at 3 nm (zoomed-in curves in Fig. 3(f)).

Light absorption and fluorescence

Spectral manifestation of ZnTPP binding to D - g - PAA and D - g - PAA / Au NPs

Fig. 4 presents the absorption spectra of ZnTPP reference ethanol solution and one mixed with water and aqueous solutions of D - g - PAA polymer and D - g - PAA / Au NPs nanohybrid. The ZnTPP ethanol solution absorption spectrum (Fig. 4(a)) has structure common to porphyrins in organic solvents [40–43]. The spectrum contains weak lower energy Q bands at 530 – 620 nm and intense higher energy B (Soret) bands at 380 – 440 nm. The multicomponent structure of Q and B bands reflects the excited electron state vibration structure. In turn, the D - g - PAA / Au NPs absorption spectrum contains the LSPR band of Au NPs with maximum at 520 nm, Fig. 4(b). Meanwhile, the D - g - PAA polymer has absorption and FL spectra in UV range that is not actual for this work.

Mixing the ZnTPP in ethanol with water causes the significant transformation of absorption spectrum, Fig. 4(a). In Fig. 4(a), the spectra are intensity normalized to see better the changes of the spectrum shape resulting from mixing. The B band intensity sharply reduces by 2.5 times. Also, the width of B band increases significantly that blurs the doublet structure of this band. Simultaneously, the weak Q bands intensity increases. Since ZnTPP molecules are hydrophobic, the observed changes in absorption spectrum are most probably caused

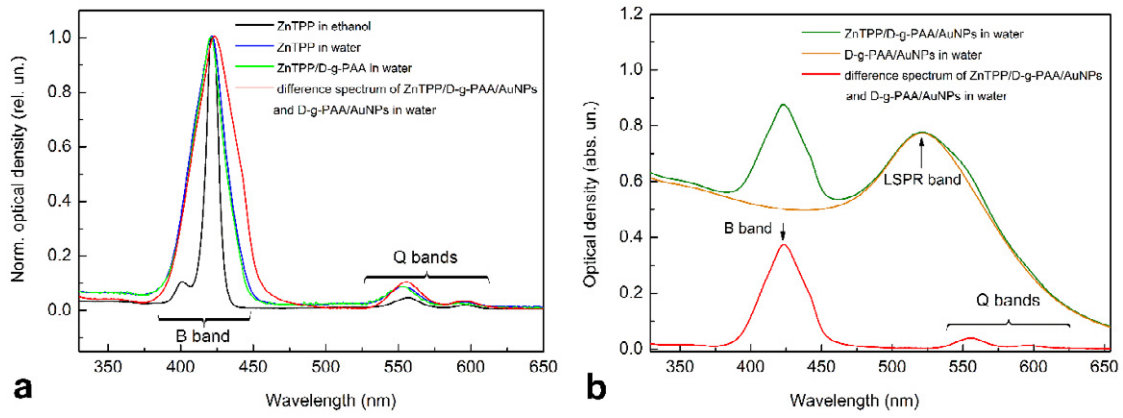

Fig. 4. (a) – Normalized absorption spectra of ZnTPP in ethanol and ZnTPP in ethanol mixed with water, D - g - PAA aqueous solution, and D - g - PAA / Au NPs aqueous solution. (b) – Normalized absorption spectrum of ZnTPP / D - g - PAA / Au NPs solution and difference spectrum of ZnTPP / D - g - PAA / Au NPs and D - g - PAA / Au NPs solutions. The difference spectrum is presented to subtract the Au NPs absorption. The concentrations: ZnTPP – 0.001 g/L, D - g - PAA – 0.080 g/L, Au – 0.079 g/L.

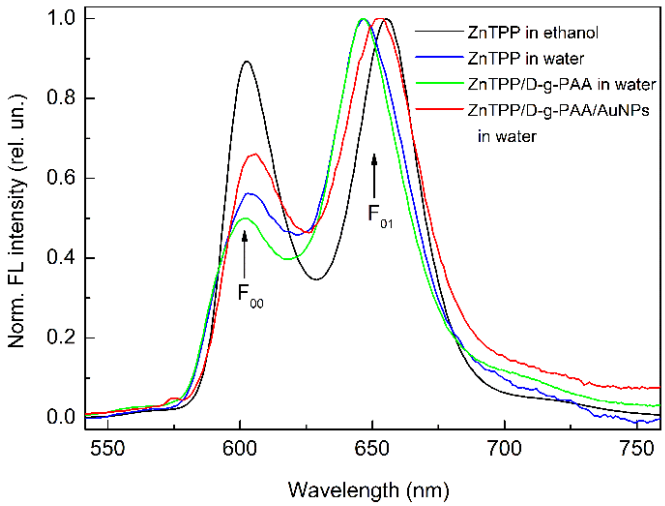

Fig. 5. Normalized fluorescence spectra of ZnTPP in ethanol and ZnTPP in ethanol mixed with water, D - g - PAA aqueous solution, and D - g - PAA / Au NPs aqueous solution. Excitation: 421 nm; concentrations: ZnTPP – 0.001 g/L, D - g - PAA – 0.080 g/L, Au – 0.079 g/L.

by their aggregation in aqueous environment. This conclusion on the formation of ZnTPP aggregates is fully consistent with the DLS results showing the presence of 32 nm radius ZnTPP aggregates in water, Fig. 3(b).

Mixing the ZnTPP in ethanol with the D - g - PAA aqueous solution does not cause any noticeable changes in the shape of absorption spectrum comparing to water case. This observation takes place in full range of polymer concentrations studied in present work. However, the mixing with polymer solution cause an increase of the absorption spectrum intensity with increasing polymer concentration that is discussed below. Finally, the mixing the ZnTPP with the D - g - PAA / Au NPs hybrid aqueous solution was performed. The absorption spectrum of ZnTPP / D - g - PAA / Au NPs aqueous solution is presented in Fig. 4(b). Since the absorption spectra of Au NPs and ZnTPP overlap significantly, to analyze the changes in ZnTPP spectrum caused by mixing we consider the difference spectrum of ZnTPP / D - g - PAA / Au NPs and D - g - PAA / Au NPs aqueous solutions, Fig. 4(a,b). It is notable that the presence of Au NPs causes further increase of the relative intensity of weak Q bands comparing to intensity of B band that indicates the influence of Au NPs on the absorptive transitions in ZnTPP molecules. Thus, the observed changes in ZnTPP absorption spectrum at the mixing proves the binding of ZnTPP molecules to both the bare D - g - PAA polymer macromolecules and with the D - g - PAA / Au NPs hybrid ones.

Fig. 5 shows the fluorescence (FL) spectra of ZnTPP in ethanol reference solution its mixture with water and D - g - PAA and D - g - PAA / Au NPs aqueous solutions. The ZnTPP ethanol solution FL spectrum (Fig.5) has structure common to porphyrins in organic solvents [41,42]. Two bands are dominant in the spectrum, higher energy F_{00} band (602 nm) and lower energy F_{01} one (655 nm).

Similar to absorption, the mixing ZnTPP in ethanol with water leads to significant transformation of FL spectrum, Fig. 5. In Fig. 5, the spectra are intensity normalized to see better the changes in the spectrum shape resulting from mixing. FL intensity decreases sharply by 8.5 times. F_{00} band intensity decreases significantly comparing of F_{01} one. F_{01} band shifts to lower energies by 9 nm. Since ZnTPP molecules are hydrophobic, the observed changes in FL spectrum are most probably caused by their aggregation in aqueous environment. The conclusion of ZnTPP aggregation in water agrees with DLS results showing the existence of 32 nm radius ZnTPP aggregates in water. The mixing ZnTPP with D - g - PAA aqueous solution caused further decrease of F_{00} band intensity in comparison with water case, Fig. 5. In turn, ZnTPP / D - g - PAA / Au NPs FL spectrum is transformed in comparison with ZnTPP in ethanol spectrum (Fig. 5) but the transformation is significantly slighter than ones occurring at ZnTPP mixing with water and aqueous

solution of D - g - PAA. Thus, the FL spectrum transformations are different for ZnTPP in water, D - g - PAA and D - g - PAA / Au NPs aqueous solutions. Thus, the ZnTPP molecules interact with D - g - PAA and D - g - PAA / Au NPs, and the Au NPs affect the interaction.

The FL anisotropy r was measured to check an assumption the binding of ZnTPP molecules to D - g - PAA and D - g - PAA / Au NPs macromolecules. For ZnTPP in ethanol r = 0.7 % that indicates that ZnTPP molecules in ethanol move freely. However, for ZnTPP in water r = 10 %. Its reflects the decrease in the number of degrees of freedom of molecules that is caused by hydrophobic interaction of molecules with water. For ZnTPP / D - g - PAA aqueous solution r = 17 % that indicates the binding of ZnTPP molecules to D - g - PAA polymer macromolecule. For ZnTPP / D - g - PAA / Au NPs aqueous solution r = 24 % indicating that binding of ZnTPP molecules occurs most efficiently to hybrid macromolecules containing the Au NPs. The FL anisotropy measurements were carried out at the following concentrations: ZnTPP – 0.001 g/L, D - g - PAA – 0.080 g/L, Au – 0.079 g/L.

Time behavior of ZnTPP /D - g - PAA and ZnTPP /D - g - PAA / Au NPs fluorescence

The behavior of ZnTPP FL spectrum was studied in dependence of time after mixing of ZnTPP in ethanol with water and aqueous solutions of D - g - PAA and D - g - PAA / Au NPs. The obtained time dependences of FL intensity are shown in Fig. 6. After 7 days after mixing, the FL intensity quenches in time for ZnTPP in water to 0.31 compared to initial value taken as 1, Fig. 6. Such FL quenching is a result of ZnTPP molecules oxidation. Meanwhile, the mixing ZnTPP ethanol solution with D - g - PAA and D - g - PAA / Au NPs aqueous solutions initially causes an increase of FL intensity with further decrease observed for ZnTPP aqueous solution. It is most probably that initial FL rise is due to binding of ZnTPP molecules to D - g - PAA and D - g - PAA / Au NPs macromolecules. In 7 days after mixing, the FL intensity decreases to 0.64 for ZnTPP / D - g - PAA and remains 1.1 times larger for ZnTPP / D - g - PAA / Au NPs in comparison with initial values. Thus, the binding of ZnTPP molecules to D - g - PAA and D - g - PAA / Au NPs prevents the them from oxidation. Moreover, considering that FL rise time for ZnTPP / D - g - PAA / Au NPs (60 min) is larger than one for ZnTPP / D - g - PAA (30 min) and that FL intensity in 7 days after mixing is significantly higher for ZnTPP / D - g - PAA / Au NPs than for ZnTPP / D - g - PAA, we can conclude that the presence of Au NPs in nanosystem contributes considerably to protection against oxidation of PS molecules.

Concentration dependence of ZnTPP / D - g - PAA and ZnTPP / D - g - PAA / Au NPs fluorescence

To determine the mechanisms of interaction of ZnTPP with D - g - PAA and Au NPs and its

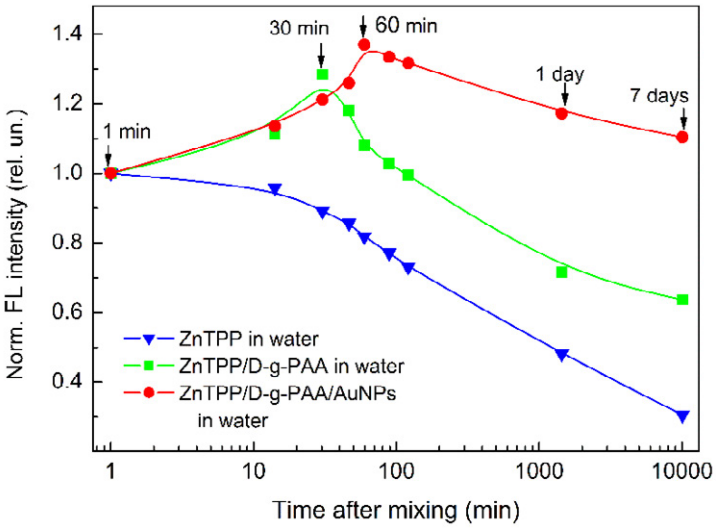

Fig. 6. Dependence of normalized FL intensity of ZnTPP on time elapsed after mixing with D - g - PAA aqueous solution and D - g - PAA / Au NPs aqueous solution. The FL intensity are normalized to the respective value at 1 min after mixing. The concentrations: ZnTPP – 0.001 g/L, D - g - PAA – 0.080 g/L, Au – 0.079 g/L. The experimental points are spline-interpolated for convenience.

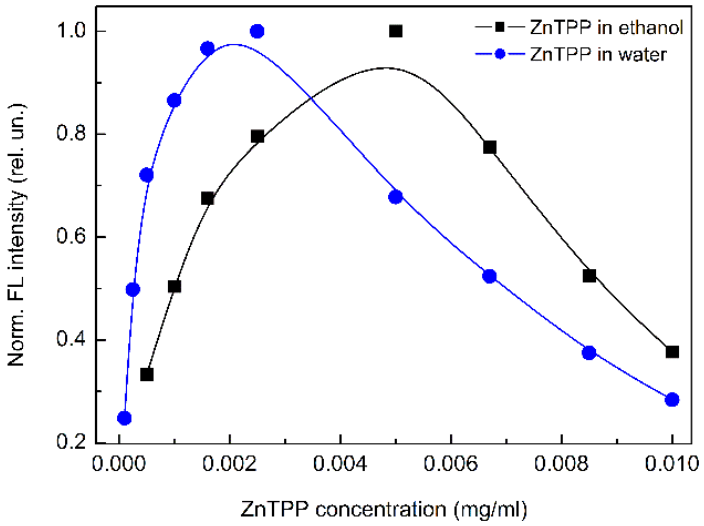

Fig. 7. Dependence of the normalized total fluorescence intensity on ZnTPP concentration for ZnTPP in ethanol and ZnTPP in ethanol mixed with water. The experimental points are spline-interpolated for convenience.

influence on electronic processes in ZnTPP molecules, the dependence of the optical properties of the hybrid nanosystem on the concentration of its components was analyzed. First, the dependence of FL intensity of ZnTPP in ethanol solution and in its mixture with water on ZnTPP concentration was studied, Fig. 7. For ZnTPP ethanol solution, a non-monotonic dependence of FL intensity was obtained, Fig. 7. Namely, the FL intensity increases at the increase in concentration, reaching a maximum at a concentration of 0.005 g/L, and then decreases at the further increase in concentration. Obviously, the ZnTPP molecules aggregation at high concentrations is a cause of the non-monotonic dependence. As for the ethanol solution of ZnTPP, the concentration dependence for ZnTPP aqueous solution is non-monotonic with a maximum at 0.0025 g/L, Fig. 7. The lower maximum concentration for ZnTPP in water can be explained by the hydrophobicity of ZnTPP molecules, which promotes the aggregation. Therefore, in subsequent measurements we used a ZnTPP concentration of 0.001 g/L, which corresponds to the middle of the linear region of the growing part of the concentration dependence for ZnTPP in water. This concentration is quite low, which ensures the absence of aggregation.

Next, the dependences of the ZnTPP FL total intensity of on the concentration of polymer and Au NPs in ZnTPP / D - g - PAA and ZnTPP / D - g - PAA / Au NPs were investigated, Fig. 8. In Fig. 8, FL intensity for different concentrations is normalized to the value of FL intensity for ZnTPP in water. Due to the significant spectral overlap of the absorption spectrum of Au NPs and the FL spectrum of ZnTPP (Figs. 4 (b) and 5), Au NPs partially absorb the photons of ZnTPP fluorescence. Therefore, the measured FL intensity is attenuated as $I(\lambda)=I_0(\lambda)10^{-D(\lambda)}$, where $I_0(\lambda)$ is the real FL intensity, and $D(\lambda)$ is the sample optical density related to the light absorption by Au NPs. Thus, the real FL intensity, which is presented in Fig. 8 by circles, was calculated as $I_0(\lambda)=10^{D(\lambda)}I(\lambda)$, where all values are taken at the appropriate gold concentrations.

It was obtained that the increase in the D - g - PAA concentration in the range of 0 – 0.2 g/L leads to a monotonic increase in the FL intensity for ZnTPP / D - g - PAA by 2.3 times, Fig. 8. Such pronounced dependence proves above conclusion on the binding of ZnTPP molecules to D - g - PAA macromolecules. Meanwhile, the dependence of FL intensity for ZnTPP / D - g - PAA / Au NPs solution on the Au concentration is non-monotonic, Fig. 8. The FL quenches by 2.2 times at the Au concentrations of 0 – 0.004 g/L, reaches maximum, and decreases to 1.25 at the increase in Au concentration up to 0.2 g/L. The fluorescence of ZnTPP molecules in ZnTPP / D - g - PAA / Au NPs nanosystem is affected by both the polymer and the Au NPs. The contribution of Au NPs was determined by division of the

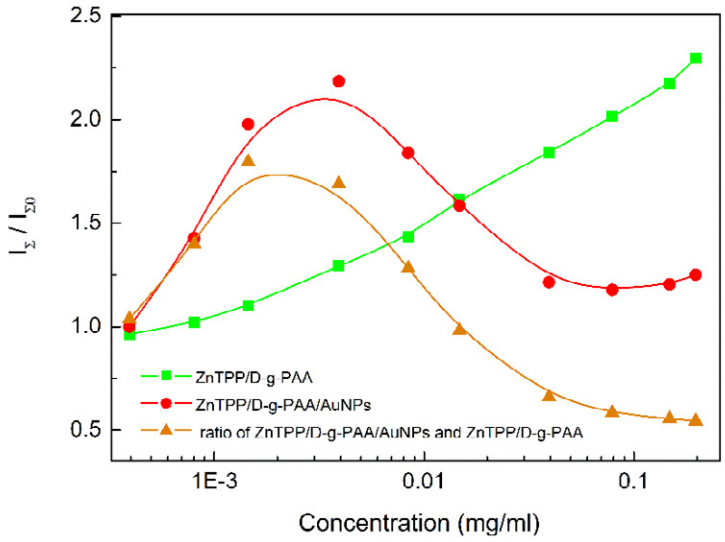

Fig. 8. Concentration dependence of normalized total FL intensity of ZnTPP in ethanol mixed with aqueous solutions of D - g - PAA and D - g - PAA / Au NPs. Triangles show the ratio of the respective concentration dependences for ZnTPP / D - g - PAA / Au NPs and ZnTPP / D - g - PAA characterizing the influence of Au NPs on absorption and PL of ZnTPP in the triple hybrid nanosystem. The FL intensity is normalized to the respective value for ZnTPP in water. The squares present the dependence on polymer concentration, the circles and triangles – the dependence on gold concentration. ZnTPP concentration – 0.001 g/L. The experimental points are spline-interpolated for convenience.

concentration dependence for ZnTPP / D - g - PAA / Au NPs by the respective dependence for ZnTPP / D - g – PAA, Fig. 8. The FL intensity increases by 1.8 times in the range of Au concentration of 0 – 0.002 g/L, reaches maximum, and then decrease to 0.5 at further increase of the concentration up to 0.2 g/L. The strong dependence of FL intensity on Au concentration indicates that ZnTPP molecules and Au NPs are close spatially located inside the D - g - PAA macromolecule due to the binding of photosensitizer molecules to the D - g - PAA / Au NPs macromolecule.

Let us consider the mechanisms which cause the influence of Au NPs on the ZnTPP fluorescence, Fig. 8. A change in the gold concentration in the sample changes the average distance between the Au NPs and the ZnTPP molecules bound to the polymer macromolecule. The distance change leads to a change in the coupling strength of surface plasmons in metal NPs with electronic excitations in molecules [44–49]. In addition, the coupling strength is affected by the spectral overlap of the LSPR in metal NP and the electronic energy spectrum of the molecule. Less distance and/or larger spectral overlap results in stronger coupling. As noted above, in the ZnTPP / D - g - PAA / Au NPs, the average distance between ZnTPP molecules and Au NPs is quite small. In addition, there is a significant spectral overlap between LSPR in Au NPs (Fig. 4 (b)) and the absorption (Fig. 4) and FL (Fig. 5) spectra of ZnTPP molecules. Therefore, a strong ZnTPP – Au NPs coupling is highly expected for the ZnTPP / D - g - PAA / Au NPs system.

Two competing physical mechanisms determine the dependence of intensity of molecule fluorescence on the distance between molecule and metal NP. The first mechanism is the plasmonic enhancement, which becomes stronger with the shortening of molecule–metal NP distance [44–49,50]. The amplitude of the plasmon field increases at the shortening distance from the metal NP as R^{-3} [49,50]. The second one is the Förster resonance energy transfer (FRET). At the FRET, the energy of an excited donor (molecule) is transferred non-radiatively to acceptor (metal NP) through dipole-dipole coupling [44–46,50,51] that results in FL quenching. The FRET quenching rate depends on the donor-acceptor distance as $\gamma_{FRET} \propto R^{-6}$ [51]. This fact limits the transfer of energy through the FRET mechanism to a range of distances less than 10 nm. The consequence of influence of these two competing mechanisms on the FL intensity is the existence of an optimal molecule-metal NP distance

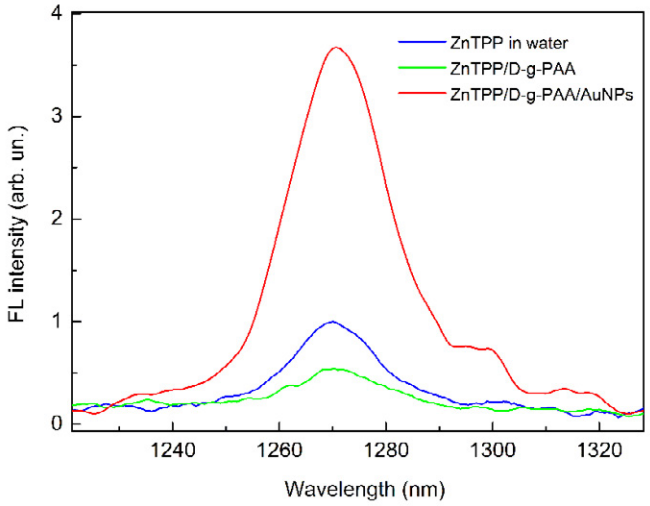

Fig. 9. Singlet oxygen emission spectra of ZnTPP in water as well as in ZnTPP / D - g - PAA and ZnTPP / D - g - PAA / Au NPs aqueous solutions. Excitation: 553 nm; concentrations: ZnTPP – 0.01 g/L, D - g - PAA – 0.080 g/L, Au – 0.079 g/L.

(about 10 nm) providing the highest FL intensity [46]. At distances less than 10 nm, a small distance decrease causes the significant FL quenching. At distances larger than 10 nm, decreasing the distance causes the FL enhancement.

Therefore, it can be concluded that low gold concentrations in the range 0 – 0.002 g/L provide an Au NP-ZnTPP molecule distance, which is large for FRET. Therefore, in this range of concentration, increasing the gold concentration leads to stronger plasmonic enhancement. At gold concentrations higher than 0.002 g/L, the Au NP-ZnTPP molecule distance is small enough to launch the process of FRET. It leads to stronger quenching of FL at the Au concentration increase. Thus, there is an optimal Au concentration at which the strongest plasmonic enhancement of electronic processes in ZnTPP molecules take place.

Photogeneration of singlet oxygen by ZnTPP / D - g - PAA and ZnTPP / D - g - PAA / Au NPs nanosystems

An important characteristic of the efficiency of some molecular system for use in PDT is the efficiency of photogeneration of singlet oxygen. Relevant studies were performed for aqueous solutions of the studied hybrid nanosystems. Fig. 9 presents the measured spectra of singlet oxygen emission for aqueous solutions of ZnTPP / D - g - PAA and ZnTPP / D - g - PAA / Au NPs nanosystems, as well as the reference spectrum of ZnTPP in water. In all spectra, the emission peak characteristic for singlet O_2 with a maximum at about 1270 nm [23] is reliably observed. Singlet oxygen emission spectra were detected for the studied samples under excitation at 421 nm (Sore band), 553 nm and 595 nm (range of Q bands). Under excitations at 421 nm and 595 nm, the peak intensities are approximately the same for ZnTPP, ZnTPP / D - g - PAA and ZnTPP / D - g - PAA / Au NPs. Also, upon excitation of aqueous solutions of ZnTPP and ZnTPP / D - g - PAA at 553 nm, the peak intensities are close to the corresponding values obtained for excitation wavelengths of 421 nm and 595 nm. However, upon excitation of the ZnTPP / D - g - PAA / Au NPs solution at 553 nm, a significant (3.2-fold) rise in intensity of the singlet oxygen peak is observed. Considering that the wavelength of 553 nm is almost resonant with LSPR in Au NPs (520 nm), it is reasonable to conclude that such enhancement of photogeneration of singlet oxygen has a plasmonic nature. Thus, the observed plasmonic enhancement of singlet oxygen photogeneration by the hybrid nanosystem ZnTPP / D - g - PAA / Au NPs indicates its prospects for photodynamic therapy.

Antibacterial activity

No bactericidal effects were detected for D - g - PAA and ZnTPP at investigated concentrations. It is known that gold nanoparticles have an antibacterial action [52]. Incubation of *S. aureus* suspension with D - g - PAA / Au NPs at concentrations of 0.08 and 0.008 g/L for 30 min reduced the amount of CFU by 50% and 30%, respectively (Fig. 10(a)). Inactivation

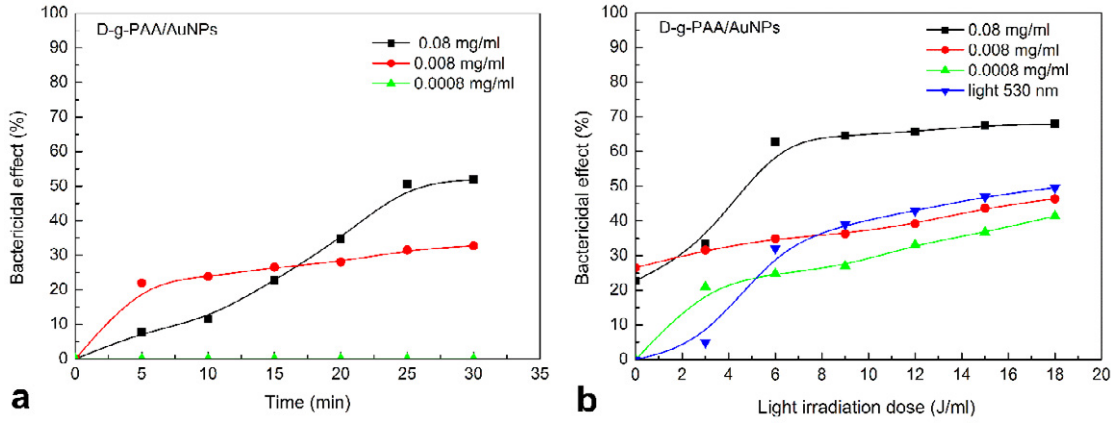

Fig. 10. Inactivation of *S. aureus* in suspension in dependence of time elapsed after adding of D - g - PAA / Au NPs (a) and 530 nm light irradiation dose (b). Concentrations: Au NPs – 0.08 g/L, 0.008 g/L, 0.0008 g/L. Light power was 0.1 J/s, irradiation dose was in the range of 3 – 18 J/mL with increments of 3 J/ml. The experimental points are spline-interpolated for convenience.

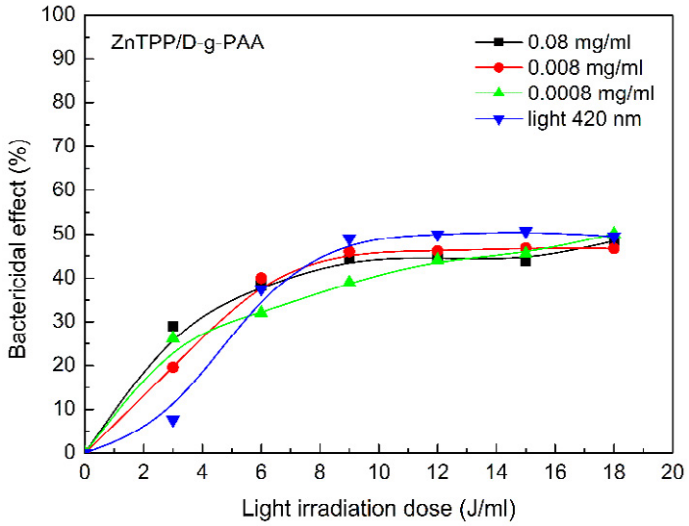

Fig. 11. Inactivation of *Staphylococcus aureus* in suspension after adding of ZnTPP / D - g - PAA and irradiation by light of 420 nm in dependence on the irradiation dose. Concentrations: D - g - PAA – 0.08 g/L, 0.008 g/L, 0.0008 g/L, ZnTPP – 0.001 g/L. Light power was 0.1 J/s, irradiation dose was in the range of 3 – 18 J/ml with increments of 3 J/mL. The experimental points are spline-interpolated for convenience.

of CFU is possible due to the penetration of gold nanoparticles into cells and blocking critical biochemical processes such as protein or ATP synthesis [53]. Lower amount of nanocomposite has no bactericidal effect.

Irradiation of the suspension by light of 530 nm inactivates 30% CFU at a dose of 6 J/mL. The effect is due to the presence of porphyrin derivatives, which are intracellular photosensitizers [54]. Only a high concentration of D - g - PAA / Au NPs 0.08 g/L increases significantly the efficiency of irradiation up to 65% of CFU inactivation (Fig. 10(b)). The effects are mediated by the ability of Au NPs to initiate the generation of free radicals including singlet oxygen. This result agrees with our above mentioned result of the enhancement of the singlet oxygen generation by nanocomposite containing the Au NPs which is most probably has the plasmonic nature. Adding of ZnTPP / D - g - PAA to the *S. aureus* suspension does not change the antibacterial activity of 420 nm light irradiation (Fig. 11). Irradiation by light in dose

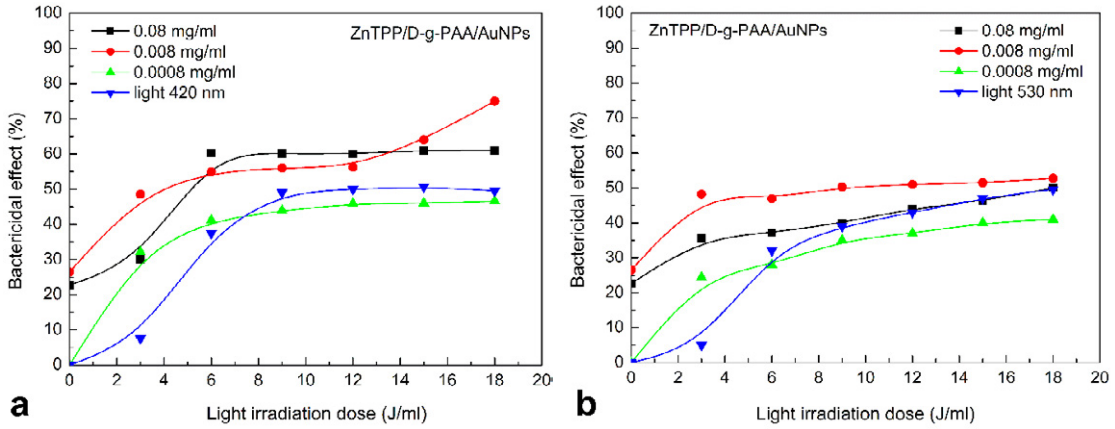

Fig. 12. Inactivation of *Staphylococcus aureus* in suspension after adding of ZnTPP / D - g - PAA / Au NPs and irradiation by light of 420 nm (a) and 530 nm (b) in dependence on the irradiation dose. Concentrations: Au NPs – 0.08 g/L, 0.008 g/L, 0.0008 g/L, ZnTPP – 0.001 g/L. Light power was 0.1 J/s, irradiation dose was in the range of 3 – 18 J/mL with increments of 3 J/mL. The experimental points are spline-interpolated for convenience.

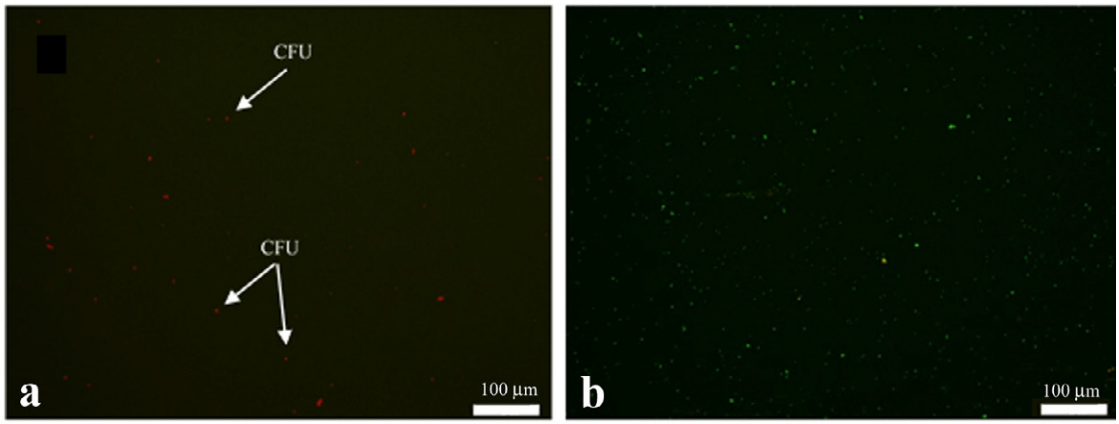

Fig. 13. Fluorescence of CFU of *S. aureus* after adding of nanocomposite ZnTPP / D - g - PAA / Au NPs (a) and staining with acridine orange (b). Concentrations: Au NPs – 0.008 g/L, ZnTPP – 0.001 g/L, acridine orange – $3.5 \cdot 10^{-3}$ M. Photo parameters: exposure time – 100 ms (a), 15 ms (b), excitation wavelength – 435-480 nm (blue optical filter).

of 3 J/mL promotes faster inactivation of CFU in the presence of photosensitizer. The process was not influenced by D - g - PAA amount. The bactericidal action of ZnTPP / D - g - PAA / Au NPs with irradiation by light of 420 nm has high efficiency at dose of 3 J/mL. The amount of CFUs is reduced by 30% for gold concentrations of 0.08 and 0.0008 g/L, and 50% for 0.008 g/L (Fig. 12(a)). The results indicate the importance of components ratio in the nanocomposite. It should be noted that at 0.008 g/L of Au NPs there possibly were two parallel processes. A light irradiation dose of 3 J/ml is sufficient for these. Other reactions that accompany the interaction of the photosensitizer and gold require more energy. This also inactivates bacteria, but requires more light irradiation. Similar results were obtained when bacterial suspension was irradiated by 530 nm light (Fig. 12(b)). Thus, the optimal Au NPs concentration is 0.008 g/L.

Red fluorescence of CFU was detected after adding of 0.008 g/L ZnTPP / D - g - PAA / Au NPs (Fig. 13(a)). Such fluorescence is the light emission from the photosensitizer molecules penetrated into the bacterial cells as part of the ZnTPP / D - g - PAA / Au NPs nanocomposite. Irradiation by blue light of a fluorescent microscope broadband light filter promotes the appearance of red luminescence, which disappears after 3 – 5 minutes. The amount of such CFUs is a small fraction of the total (Fig. 13(b)). The detected bactericidal activity of the

solutions of our nanosystems was registered for a short time which does not exceed 20 minutes. Therefore, ZnTPP / D - g - PAA / Au NPs aqueous solutions are suitable for rapid reduction of the CFU population in the open wounds.

CONCLUSIONS

In conclusion, the ZnTPP / D - g - PAA / Au NPs hybrid nanosystem aqueous solution was synthesized for potential use in photodynamic therapy. The polymer Dextran-graft- Polyacrylamide copolymer (D - g - PAA) macromolecules with dextran core and 10 PAA grafted chains were used as the matrix for gold NPs synthesis and for further ZnTPP / D - g - PAA / Au NPs triple nanosystem fabrication. The morphology study of ZnTPP / D - g - PAA / Au NPs in water by mean of DLS method showed the system to be aggregatively and sedimentationally stable during several days after preparation. The mixing of the ZnTPP in ethanol with the D - g - PAA and D - g - PAA / Au NPs aqueous solutions causes the optical density increase as well as the FL intensity increase and the transformation of the shape of fluorescence spectrum of ZnTPP comparing to changes occurring at the mixing of the ZnTPP in ethanol with water. The obtained results prove the fact of the binding of ZnTPP molecules both to D - g - PAA and D - g - PAA / Au NPs macromolecules. It was proved that ZnTPP molecules bind best to macromolecules which contain the Au NPs.

The dependence of fluorescence intensity of ZnTPP in ZnTPP / D - g - PAA / Au NPs on the gold concentration is non-monotonic with 2.2 times enhancement in maximum at Au concentration of about 0.005 g/L. Such dependence is due to competing action of surface plasmon enhancement and FRET mechanisms. As a result, there is an optimal gold concentration providing the strongest plasmonic enhancement of electronic processes in ZnTPP molecules take place. The 3.2 times plasmon enhancement of singlet oxygen photogeneration under excitation resonant with LSPR in Au NPs was revealed for ZnTPP / D - g - PAA / Au NPs system, which indicates its promise for PDT applications.

The high bactericidal efficiency of ZnTPP / D - g - PAA / Au NPs aqueous solution at light irradiation was revealed for *Staphylococcus aureus* wild strains. The ZnTPP / D - g - PAA / Au NPs aqueous solution with 0.08 g/L gold concentration at surface plasmon resonant light irradiation provides the rapid (up to 20 min) inactivation up to 65% of colony-forming units (CFU) of *S. aureus*. Such rapid high bactericidal efficiency was explained as an ability of Au NPs to initiate the generation of singlet oxygen. Respectively, ZnTPP / D - g - PAA / Au NPs aqueous solutions are suitable for rapid reduction of the CFU population in the open wounds.

ACKNOWLEDGMENTS

This work was supported by National Research Foundation of Ukraine Project (No. 2020.02/0022) and Ministry of Education and Science of Ukraine Project (No. 0122U001818),

CONFLICTS OF INTEREST

The authors declare that there are no conflicts of interest.

REFERENCES

1. Ghorbani J, Rahban D, Aghamiri S, Teymouri A, Bahador A. Photosensitizers in antibacterial photodynamic therapy: an overview. Laser Therapy. 2018; 4: 293–302.
2. Abrahamse H, Hamblin MR. New photosensitizers for photodynamic therapy. Biochemical Journal. 2016; 473: 347–364.
3. Jori G, Fabris C, Soncin M, Ferro S, Coppellotti O, Dei D, Fantetti L, Chiti G, Roncucci G. Photodynamic therapy in the treatment of microbial infections: Basic principles and perspective applications. Lasers in Surgery and Medicine. 2006; 38: 889–905.
4. Huang L, Xuan Y, Koide Y, Zhiyentayev T, Tanaka M, Hamblin MR. Type I and type II mechanisms of antimicrobial photodynamic therapy: An in vitro study on gram-negative and gram-positive bacteria. Lasers in Surgery and Medicine. 2012; 44: 490.
5. Martinez De Pinillos Bayona A, Mroz P, Thunshelle C, Hamblin MR. Design features for optimization of tetrapyrrole macrocycles as antimicrobial and anticancer photosensitizers. Chemical Biology and Drug Design. 2017; 89: 192–206.
6. Lin Y, Zhou T, Bai R, Xie Y. Chemical approaches for the enhancement of porphyrin skeleton-based photodynamic therapy. Journal of Enzyme Inhibition and Medicinal Chemistry. 2020; 35: 1080–1099.
7. Zhang Z, Yu HJ, Wu S, Huang H, Si LP, Liu HY, Shi L, Zhang HT. Synthesis, characterization, and photodynamic therapy activity of 5,10,15,20-tetrakis(carboxyl)porphyrin. Bioorganic and Medicinal Chemistry. 2019; 27: 2598–2608.
8. Elms J, Beckett PN Griffin P, Curran AD. Mechanisms of isocyanate sensitisation. An in vitro approach. Toxicology in Vitro. 2001; 15: 631.
9. Milacic V, Dou QP. The tumor proteasome as a novel target for gold(III) complexes: implications for breast cancer therapy. Coordination Chemistry Reviews. 2009; 19: 398–403.
10. Lammer AD, Cook ME, Sessler JL. Synthesis and anti-cancer activities of a water soluble gold(III) porphyrin. Journal of Porphyrins and Phthalocyanines. 2015; 19: 398–403.

11. Shamaila S, Zafar N, Riaz S, Sharif R, Nazir J, Naseem S. Gold nanoparticles: an efficient antimicrobial agent against enteric bacterial human pathogen. Nanomaterials. 2016; 6: 71.
12. Kutsevol N, Harahuts Y, Shton I, Borikun T, Storchai D, Lukianova N, Chekhun V. In vitro study of toxicity of hybrid gold-polymer composites. Molecular Crystals and Liquid Crystals. 2018; 671: 1–8.
13. Yeshchenko OA, Kutsevol NV, Naumenko AP. Light-induced heating of gold nanoparticles in colloidal solution: dependence on detuning from surface plasmon resonance. Plasmonics. 2016; 11: 345–350.
14. Yeshchenko OA, Kozachenko VV Light-induced heating of dense 2D ensemble of gold nanoparticles: Dependence on detuning from surface plasmon resonance. Journal of Nanoparticle Research. 2015; 17: 296.
15. Harahuts YI, Pavlov VA, Mokrinskaya EV, Chuprina NG, Davidenko NA, Naumenko AP, Bezugla TM, Kutsevol NV. The study of Au sol synthesized in uncharged and charged star-like copolymers under light irradiation. Functional Materials. 2019; 4: 723–728.
16. Kutsevol N, Kuziv Y, Bezugla T, Virych P, Marynin A, Borikun T, Lukianova N, Virych P, Chekhun V. Application of new multicomponent nanosystems for overcoming doxorubicin resistance in breast cancer therapy. Applied Nanoscience. 2021; https://doi.org/10.1007/s13204-020-01653-y.
17. Millenbaugh NJ, Baskin JB, DeSilva MN, Elliot WR, Glickman RD. Photothermal killing of Staphylococcus aureus using antibody-targeted gold nanoparticles. International Jpurnal of Nanomedicine. 2015; 10: 1953–1960.
18. Lim ZZJ, Li JEJ, Ng CT, Yung LYL, Bay BH. Gold nanoparticles in cancer therapy. Acta Pharmacologica Sinica. 2011; 32: 983–990.
19. Von Maltzahn G, Park JH, Lin KY, Singh N, Schwöppe C, Mesters R, Berdel WE, Ruoslahti E, Sailor MJ, Bhatia SN. Nanoparticles that communicate in vivo to amplify tumour targeting. Nature Materials. 2011; 10: 545–552.
20. Yu H, Peng Y, Yang Y, Li ZY. Plasmon-enhanced light–matter interactions and applications. npj Computational Materials. 2019; 5: 45.
21. Baumberg JJ, Aizpurua J, Mikkelsen MH, Smith DR. Extreme nanophotonics from ultrathin metallic gaps. Nature Materials. 2019; 18: 668–678.
22. Hou W, Cronin SB. A review of surface plasmon resonance-enhanced photocatalysis. Advanced Functional Materials. 2013; 23: 1612–1619.
23. Zhang Y, Aslan K, Previte MJR, Geddes CD. Metal-enhanced singlet oxygen generation: a consequence of plasmon enhanced triplet yields. Journal of Fluorescence. 2007; 17: 345–349.
24. Macia N, Kabanov V, Côté-Cyr M, Heyne B. Roles of near and far fields in plasmon-enhanced singlet oxygen production. Journal of Physical Chemistry Letters. 2019; 10: 3654–3660.
25. Macia N, Kabanov V, Heyne B. Rationalizing the plasmonic contributions to the enhancement of singlet oxygen production. The Journal of Physical Chemistry C. 2020; 124: 3768–3777.
26. Planas O, Macia N, Agut M, Nonell S, Heyne B. Distance-dependent plasmon-enhanced singlet oxygen production and emission for bacterial inactivation. Journal of the American Chemical Society. 2016; 138: 2762–2768.
27. Tavakkoli Yaraki M, Daqiqeh Rezaei S, Tan YN. Simulation guided design of silver nanostructures for plasmon-enhanced fluorescence singlet oxygen generation and SERS applications. Physical Chemistry Chemical Physics. 2020; 22: 5673–5687.
28. Mohamed MM, Fouad SA, Elshoky HA, Mohammed GM, Salaheldin TA. Antibacterial effect of gold nanoparticles against corynebacterium pseudotuberculosis. International Journal of Veterinary Science and Medicine. 2017; 5: 23–29.
29. Khosravi H, Hashemi B, Rahmani F, Gel dosimetry: The effect of gold nanoparticles on the dose enhancement in the external radiation therapy. Nanomedicine Research Journal. 2016; 1: 31–38.
30. Khosravi H, Mahdavi Gorabi A, Rahmani F, Ebadi A, The impact of nano-sized gold particles on the target dose enhancement based on photon beams using by Monte Carlo method. Nanomedicine Research Journal. 2016; 1: 84–89.
31. Zabihzadeh M, Moshirian T, Ghorbani M, Knaup C, Behrooz MA, A Monte Carlo study on dose enhancement by homogeneous and inhomogeneous distributions of gold nanoparticles in radiotherapy with low energy X-rays. Journal of Biomedical & Physics Engineering. 2018; 8: 13–28.
32. Karabasz A, Bzowska M, Szczepanowicz K. Biomedical applications of multifunctional polymeric nanocarriers: a review of current literature. International Journal of Nanomedicine. 2020; 15: 8673–8696.
33. Kutsevol NV, Chumachenko VA, Harahuts II, Marinin AI. Aging process of gold nanoparticles synthesized in situ in water solutions of polyacrylamides. Mukbanianym OV, Abadie MJ, Tatrishvili T, editors. Chemical Engineering of Polymers. Production of Functional and Flexible Materials, Apple Academic Press; 2017: 119–129.
34. Bulavin L, Kutsevol N, Chumachenko V, Soloviov D, Kuklin A, Marynin A. SAXS combined with UV-Vis spectroscopy and QELS: Accurate characterization of silver sols synthesized in polymer matrices. Nanoscale Research Letters. 2016; 11: 35.
35. Chumachenko V, Kutsevol N, Harahuts Y, Rawiso M, Marinin A, Bulavin L. Star-like dextran-graft-PNIPAM copolymers. Effect of internal molecular structure on the phase transition. Journal of Molecular Liquids. 2017; 235: 77–82.
36. Deng S, Gigliobianco MR, Censi R, Di Martino P. Polymeric nanocapsules as nanotechnological alternative for drug delivery system: current status, challenges and opportunities. Nanomaterials, 2020; 10: 847.
37. Chumachenko VA, Shton IO, Shishko ED, Kutsevol NV, Marinin AI, Gamaleia NF. Branched copolymers dextran-graft-polyacrylamide as nanocarriers for delivery of gold nanoparticles and photosensitizers to tumor cells. Fesenko O, Yatsenko L, editors. Nanophysics Nanophotonics Surface Studies and Applications, Springer Proceedings in Physics series, Springer; 2016: 379–390.
38. Kutsevol NV, Chumachenko VA, Rawiso M, Shkodich VF, Stoyanov OV. Star-like dextran-polyacrylamide polymers: prospects of use in nanotechnologies. Journal of Structural Chemistry. 2015; 56: 1016–1023.
39. Yuan X, Liu Z, Wang Y, Xu Y, Zhang W, Mu T. The non-negative truncated singular value decomposition for adaptive sampling of particle size distribution in

dynamic light scattering inversion. Journal of Quantitative Spectroscopy and Radiative Transfer. 2020; 246: 106917.
40. Marsh DF, Mink LM. Microscale synthesis and electronic absorption spectroscopy of tetraphenylporphyrin H2(TPP) and metalloporphyrins ZnII(TPP) and NiII(TPP). Journal of Chemical Education. 1996; 73: 1181.
41. Strachan JP, Gentemann S, Seth J, Kalsbeck WA, Lindsey JS, Holten D, Bocian DF. Effects of orbital ordering on electronic communication in multiporphyrin arrays. Journal of the American Chemical Society. 1997; 119: 11191–11201.
42. Harriman A. Luminescence of porphyrins and metalloporphyrins. Part 1 – Zinc(II) nickel(II) and manganese(II) porphyrins. Journal of the Chemical Society Faraday Transactions 1: Physical Chemistry in Condensed Phases. 1980; 6: 1978–1985.
43. Nguyen KA, Day PN, Pachter R, Tretiak S, Chernyak V, Mukamel S. Analysis of absorption spectra of zinc porphyrin, zinc meso-tetraphenylporphyrin and halogenated derivatives. Journal of Physical Chemistry A. 2002; 106: 10285–10293.
44. Törmö P, Barnes WL. Strong coupling between surface plasmon polaritons and emitters: A Review. Reports on Progress in Physics. 2015; 78: 013901.
45. Rodarte AL, Tao AR. Plasmon-exciton coupling between metallic nanoparticles and dye monomers. Journal of Physical Chemistry C. 2017; 121: 3496–3502.
46. Anger P, Bharadwaj P, Novotny L. Enhancement and quenching of single-molecule fluorescence. Physical Review Letters. 2006; 96: 113002.
47. Yeshchenko OA, Khort PS, Kutsevol NV, Prokopets VM, Kapush O, Dzhagan V. Temperature driven plasmon-exciton coupling in thermoresponsive dextran-graft-PNIPAM/Au nanoparticle/CdTe quantum dots hybrid nanosystem. Plasmonics. 2021; 16: 1137–1150.
48. Roller EM, Argyropoulos C, Högele A, Liedl T, Pilo-Pais M. Plasmon-exciton coupling using DNA templates. Nano Letters. 2016; 16: 5962–5966.
49. Dolinnyi AI. Nanometric rulers based on plasmon coupling in pairs of gold nanoparticles. Journal of Physical Chemistry C. 2015; 119: 4990–5001.
50. Su Q, Jiang C, Gou D, Long Y. Surface plasmon-assisted fluorescence enhancing and quenching: from theory to application. ACS Applied Bio Materials. 2021; 4: 4684–4705.
51. Medintz I, Hildebrandt N. FRET - Förster resonance energy transfer: From theory to applications. Wiley; 2013.
52. Vimbela GV, Ngo SM, Fraze C, Yang L, Stout DA. Antibacterial properties and toxicity from metallic nanomaterials. International Journal of Nanomedicine. 2017; 12: 3941–3965.
53. Cui Y, Zhao Y, Tian Y, Zhang W, Lü X, Jiang X. The molecular mechanism of action of bactericidal gold nanoparticles on Escherichia Coli. Biomaterials. 2012; 33: 2327–2333.
54. Fyrestam J. Porphyrins and heme in microorganisms – porphyrin content and its relation to phototherapy and antimicrobial treatments in vivo and in vitro. Stockholm University; 2017.